



Water in clinopyroxene from the 2021 Geldingadalir eruption of the Fagradalsfjall Fires, SW-Iceland

Ioana-Bogdana Radu¹ · Henrik Skogby¹ · Valentin R. Troll^{2,3} · Frances M. Deegan^{2,3} · Harri Geiger⁴ · Daniel Müller⁵ · Thor Thordarson⁶

Received: 30 November 2022 / Accepted: 25 March 2023
© The Author(s) 2023

Abstract

Water content plays a significant role in magma genesis, ascent rate, and, ultimately, in the style and intensity of volcanic eruptions, due to its control on the density, viscosity and melting behaviour of silicate melts. A reliable method for determining the pre-eruptive magmatic water content is to use phenocrysts of nominally anhydrous minerals (NAMs) which can preserve water as hydrogen configurations in structural defects. The advantage of this method is that eruptive changes such as water loss during magma degassing may be experimentally reconstructed and analysed by infrared spectroscopy. Applying this to clinopyroxene crystals ($n=17$) from lava samples ($n=7$) from April 2021 of the Geldingadalir eruption, SW-Iceland, reveals parental water contents of 0.69 ± 0.07 to 0.86 ± 0.09 wt. % H_2O . These values are higher than those expected for typical mid-ocean ridge basalts (MORB 0.3–0.5 wt. % on average) indicating a significant plume (OIB) contribution to the magma source. Moreover, such water concentrations would imply that water saturation in the ascending Geldingadalir magmas was attained only at very shallow levels within the plumbing system. This could explain the at times pulsating behaviour within the uppermost conduit system as being the result of shallow episodic water vapour exsolution in addition to the deep-sourced CO_2 flux.

Keywords Water in nominally anhydrous minerals · Clinopyroxene phenocrystals · Pulsating eruption · Shallow magma degassing · Geldingadalir

Editorial responsibility: N. Métrich

This paper constitutes part of a topical collection: Low intensity basalt eruptions: the 2021 Geldingadalir and 2022 Meradalir eruptions of the Fagradalsfjall Fires, SW Iceland

✉ Ioana-Bogdana Radu
bogdana.radu@nrm.se

¹ Department of Geosciences, Swedish Museum of Natural History, Box 50007, SE-104 05 Stockholm, Sweden

² Dept. of Earth Sciences, Natural Resources & Sustainable Development, Uppsala University, Uppsala, Sweden

³ Centre of Natural Hazard and Disaster Science (CNDS), Uppsala University, Uppsala, Sweden

⁴ Institute of Earth and Environmental Sciences, University of Freiburg, Freiburg im Breisgau, Germany

⁵ GFZ German Research Centre for Geosciences, Potsdam, Germany

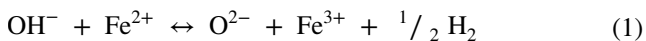
⁶ Faculty of Earth Sciences, University of Iceland, Reykjavík, Iceland

Introduction

The amount of water in silicate melts influences their crystallisation and melting temperatures, density, and viscosity, all of which exert a fundamental control on magma differentiation, ascent, and the explosivity of volcanic eruptions (Cashman 2004; Edmonds and Wallace 2017; Ferguson et al. 2016; Gonnermann and Manga 2013; La Spina et al. 2022; Preece et al. 2016; Roggensack et al. 1997; Woods and Koyaguchi 1994). Quantifying the magmatic water content of past and present eruptions, with respect to their geodynamic setting, is key in understanding future volcanic eruptions and predicting their eruptive behaviour (Cassidy et al. 2019; Marti and Folch 2005; Wallace et al. 2015). There are various methods that can be used for determining the pre-eruptive water content of magmas. Commonly, these rely on volatile contents of naturally or artificially quenched volcanic glasses (Malfait et al. 2014), or on melt inclusions trapped in phenocrysts (Métrich and Wallace 2008; Petrelli et al. 2018; Sides et al. 2014); however, these may be affected by complex degassing, or are absent from samples (Dixon et al. 1997). Alternatively, the initial magmatic water

content can be determined by plagioclase-liquid hygrometry (Lange et al. 2009) or by using phenocrysts of nominally anhydrous minerals (NAMs) such as clinopyroxene (Aubaud et al. 2004; Lloyd et al. 2016; Wade et al. 2008; Weis et al. 2015).

Clinopyroxene may incorporate water (as hydrogen) during magma crystallisation, through structural defects compensated by M2 cation vacancies or charge deficient substitutions (e.g. ${}^{\text{IV}}\text{Al}^{3+} + \text{H}^+ \leftrightarrow \text{Si}^{4+}$). However, the preservation of hydrogen in NAMs is challenged by its high mobility as a function of pressure, temperature, oxygen fugacity, and water activity (Hercule and Ingrin 1999; Ingrin and Skogby 2000; Skogby et al. 1990). Studies on intracrystalline hydrogen diffusivity show that it will attain equilibrium within minutes to hours in clinopyroxene with $X_{\text{Fe}/(\text{Fe}+\text{Mg})} > 0.07$, with kinetics similar to those of H-D exchange (Ingrin and Blanchard 2006). The outward hydrogen diffusion, during rehydration and dehydration processes, were shown to rely on the ferric to ferrous iron content and to follow the reversible redox reaction (Skogby and Rossman 1989):



During magma ascent and degassing, fluid pressure decreases, and NAMs may lose their hydrogen content in part or entirely (Hamada et al. 2011; Johnson et al. 2010; Preece et al. 2016). Depending on the eruption style and cooling speed, slow-crystallising lavas may suffer similar hydrogen loss (Wade et al. 2008). However, during dehydration and cooling under such conditions, the hydrogen-associated defects are preserved as they are governed by cation and vacancy diffusion that are orders of magnitude slower than reaction (1) (Cherniak and Dimanov 2010; Ingrin and Blanchard 2006; Ingrin and Skogby 2000). This implies that clinopyroxene crystals can retain information about their initial hydrogen concentration and hence permits recalculation of parental magmatic water contents.

In this study, we use partially dehydrated clinopyroxene phenocrysts from basaltic, pahoehoe lavas emplaced within the Geldingadalir lava flow field (Fagradalsfjall Fires, Iceland) between 2 and 10 of April 2021. A total of 17 crystals were studied from 7 samples collected over four main vents. The initial water content of the clinopyroxene was restored by performing a series of rehydration experiments and was subsequently measured by Fourier transform infrared spectroscopy (FTIR). These results were used together with calculated partition coefficients between clinopyroxene and basaltic magma to determine the pre-eruptive magmatic water content and to explore its implications for the magmatic source and for the influence on eruptive style during the earlier phases of the Fagradalsfjall Fires multi-vent eruption.

Geological background

Fagradalsfjall is a hyaloclastite tuya that is part of the oblique extensional structures on Reykjanes Peninsula (Fig. 1). After a dormant period of ~780 years, a low-intensity effusive eruption started on 19 March, 2021, with the opening of several small vents along a 180-m long segment in Geldingadalir valley, SE of Fagradalsfjall (Pedersen et al. 2021). The eruption was characterised by a steady lava discharge with bubble bursting and weak fountaining activity, accompanied by low-viscosity overflows and formation of spatter cones (Bindeman et al. 2022; Halldórsson et al. 2022). Subsequently, five more vents opened from 5 to 13 April, following a N-NE trend from the central first eruption. The discharge rate increased from $6 \pm 0.5 \text{ m}^3/\text{s}$ to $9.8 \pm 0.7 \text{ m}^3/\text{s}$ and the eruption shifted to lava fountaining of variable intensities accompanied by rhythmic overflows (Bindeman et al. 2022). By 2 May, only vent 5 remained active, which progressively developed into a volcanic cone, recording the last lava flow of this eruptive episode on 18 September, 2021.

Samples

All samples from this study ($n=7$) were collected from the interiors of freshly emanated Pahoehoe-type, olivine tholeiite lava flows, and the glowing-hot sampled material was subsequently quenched in air. Except for sample Fagra 3, which was collected on the second day after the opening of the eruptive fissure, all other samples were collected on the date of the opening itself (Table 1). For the sampling period, magma discharge is estimated at $6 \pm 0.5 \text{ m}^3/\text{s}$ (Bindeman et al. 2022), with associated gas pollution, lava flow, and moss fires, corresponding to the incipient and less intense part of the eruption (phase I to phase II, Barsotti et al. (2023)). Three samples were taken from vent 1 (April 2 and 9), two samples from vent 2 (April 6 and 9), and one sample from vent 3 (April 9) and from vent 4 (April 10), respectively. The samples were selected in order to obtain a first-order estimate of magmatic water contents in the early stages of the eruption. The collected material consists mostly of finely crystalline to glassy basaltic lava, with ca. 10 vol. % visible phenocrysts comprising plagioclase, olivine, and pyroxene. The latter are the least abundant, accounting for approximately 5 to 15 vol. % of the total amount of phenocrysts in the investigated samples. In addition, clinopyroxene grain size varies considerably, from ~50 μm to > 1 mm, among the different samples as well as within individual samples. The crystals are irregularly shaped, of dark green colour and lack any obvious cracks or inclusions.

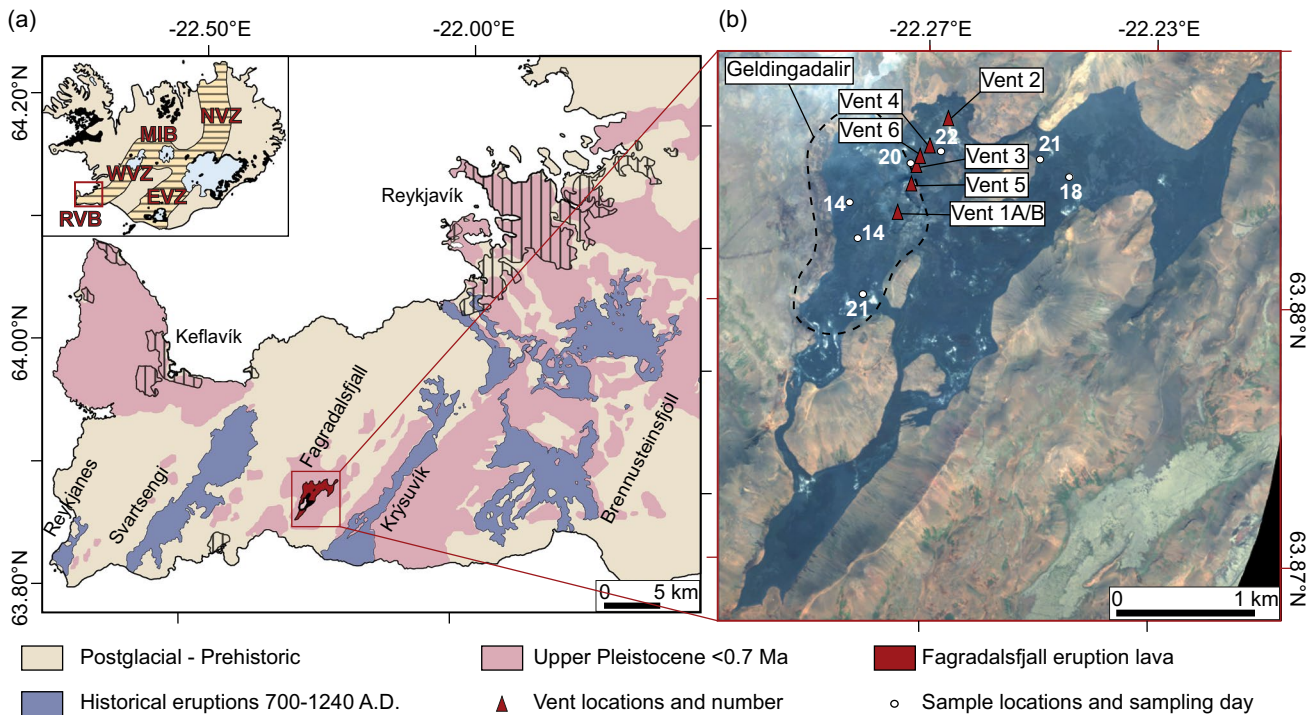


Fig. 1 The 2021 Geldingadalir eruption site on the Reykjanes Peninsula. **(a)** Insert of Iceland and main rift zones (NVZ = Northern Volcanic Zone; MIB = Mid-Iceland Belt; WVZ = Western Volcanic Zone; EVZ = Eastern Volcanic Zone; RVB = Reykjanes Volcanic Belt) and geological map of the Reykjanes Peninsula. Historical (late Holocene) eruptions are in blue (Reykjanes, Svartsengi, Fagradalsfjall, Krýsuvík, Brennisteinsfjöll), prehistoric eruptions are marked in yellow (postglacial) and pink (upper Pleistocene to early

Holocene), and the lava field from the 2021 Fagradalsfjall eruption is marked in red. **(b)** Orthophotograph (www.earth.esa.int/eogateway/missions/pleiades) corresponding to the red box in figure a. The location of sampling points is marked with white circles and numbered according to the days since the beginning of the eruption. Eruptive vents are marked with red triangles and are numbered according to the order in which they erupted. Figure after data from Bindeman et al. (2022); Einarsson (2008); and Sæmundsson (2016)

Table 1 Information regarding sample collection and analyses

Sample name	Latitude	Longitude	Eruption date	Sampling date	Sample description	Days *	No. of grains analysed
Fagra 1 (IC-GEL-PAH-Vent1-03)	63.8897	-22.2777	02 April 2021	02 April 2021	Active pahoehoe lava flow.	14	2
Fagra 2 (IC-GEL-PAH-Vent1-04)	63.8878	-22.2771	02 April 2021	02 April 2021	Active pahoehoe lava flow.	14	3
Fagra 3 (IC-GEL-PAH-Vent2-01)	63.8932	-22.2439	06 April 2021	06 April 2021	Pahoehoe lava. Taken liquid-fresh from the lava of the new fissure about one day after it opened	18	2
Fagra 4 (IC-GEL-PAH-Vent2-02)	63.8951	-22.2660	09 April 2021	09 April 2021	Active pahoehoe lava flow.	21	2
Fagra 5 (IC-GEL-PAH-Vent3-01)	63.8923	-22.2689	08 April 2021	09 April 2021	Pahoehoe lava.	20	3
Fagra 6 (IC-GEL-BLK-Vent1-05)	63.8838	-22.2755	09 April 2021	09 April 2021	Active pahoehoe lava flow.	21	3
Fagra 7 (IC-GEL-PAH-Vent4-01)	63.8931	-22.2645	10 April 2021	10 April 2021	Active pahoehoe lava flow.	22	2

Sample details from Bindeman et al. 2022

*Days since eruption start. March 19th = day zero

Methods

The lava samples were gently crushed and clinopyroxene crystals were handpicked under a binocular microscope. Two

to three grains per sample (Table 1) were chosen based on size, pristine appearance, and morphology. All crystals ($n=17$) were mounted in thermoplastic resin and based on their morphology and extinction angles were oriented along the

crystallographic *c* axis, and their (100) and (010) crystal faces (see detailed procedure in Stalder and Ludwig (2007)). Crystals were polished to a thickness of a few tens to hundreds of micrometres using Al₂O₃-grinding paper of various particle size-grade (Table 2). The clinopyroxene crystals analysed for their water content were also analysed for major element chemistry by electron micro probe analyses (EMPA). All sample preparation and analyses were carried out at the Swedish Museum of Natural History, Sweden, except for microprobe analyses, which were performed at the University of Freiburg, Germany.

Aerial UAV imaging

Video recordings of the main crater were acquired on 8 June 2021 by drone loop overflights or static hovering in the vicinity of the crater. These were captured with a standard DJI Mavic Air 2 drone quadcopter equipped with a 1/2" (1.27 cm) CMOS camera sensor and a three-axis gimbal for image stabilisation. The recordings were acquired in high-resolution 4k video format, from which frames were extracted and used to create image series. The weather conditions during drone flights were calm and sunny, and the wind direction and plume drift were considered when establishing the flight paths. Due to intense helicopter traffic, flight altitude was set unusually low (~50m above the crater), which limited

the available region from the row of craters and lava flows. The acquired images are oriented northwards, capturing the main direction of the lava flow (which was predominantly towards the south), and the pulsating behaviour at the vents.

Electron micro probe analysis

Mineral major element chemistry was acquired using a Cameca SX100 electron microprobe under standard operating conditions of 15 kV accelerating voltage and 20 nA beam current. Two spots were analysed on each crystal, with a focused beam of 1 μm diameter and 20 s counting time on peak and 10 s on background. Iron content is reported as FeO_t. The spectrometers were calibrated using diopside for Ca and Si, orthoclase for K, albite for Na, spessartine for Mn, rutile for Ti, magnesium oxide for Mg, hornblende for Al, hypersthene for Fe, and chromite for Cr. The crystals showed no marked zonation in backscattered electron (BSE) images. Standard deviations for major oxides are as follows: SiO₂ ~0.29 wt%, TiO₂ ~0.03 wt%, Al₂O₃ ~0.08 wt%, FeO ~0.25 wt%, MnO ~0.08 wt%, MgO ~0.14 wt%, CaO 0.43 wt%, Na₂O ~0.04 wt%, K₂O ~0.03 wt%, Cr₂O₃ ~0.07 wt%. Using the obtained chemical composition in oxide weight percentages, the number of atoms per formula unit was calculated based on six oxygen, four cation normalisation. Additionally, the Fe²⁺ and Fe³⁺ content was calculated using the results of the Mössbauer analyses.

Table 2 Water contents of clinopyroxene crystals from Geldingadalir lavas, before and after H₂-treatment

Sample	Water content (ppm wt. H ₂ O)			Thickness (μm) (010)/(100)
	Untreated	After H ₂ treatment (37h)	After H ₂ treatment (94h)	
Fagra 1 (1)	10	n.d.	137	480/950
Fagra 1 (2)	32	132	n.d.	270/220
Fagra 2 (1)	6	144	n.d.	195/235
Fagra 2 (2)	13	136	n.d.	155/120
Fagra 2 (3)	17	170	n.d.	160/150
Fagra 3 (1)	6	134	n.d.	355/575
Fagra 3 (2)	13	167	n.d.	225/240
Fagra 4 (1)	9	125	n.d.	230/385
Fagra 4 (2)	17	149	n.d.	270/450
Fagra 5 (1)	11	119	n.d.	315/285
Fagra 5 (2)	12	119	n.d.	270/435
Fagra 5 (3)	27	141	n.d.	365/190
Fagra 6 (1)	8	132	n.d.	220/360
Fagra 6 (2)	7	142	n.d.	360/290
Fagra 6 (3)	11	108	n.d.	205/200
Fagra 7 (1)	21	175	n.d.	285/84
Fagra 7 (2)	18	131	n.d.	190/280

n.d. not determined

Rehydration experiments

Hydrogen-associated defects in oriented clinopyroxene were experimentally refilled by placing the crystals in a gold sample holder and introducing them into a horizontal glass-tube furnace, where they were kept under a stream of H₂ gas at 700 °C and 1atm. The temperature was controlled with a Pt₁₀₀-Pt₉₀Rh₁₀ thermocouple placed directly above the samples, in the middle of the furnace, with an estimated uncertainty of ±2 °C. Prior to introducing the samples, the medium inside the furnace was preconditioned under a flux of CO₂ gas, to prevent any reaction between the crystals and ambient O₂, or an explosion when introducing the H₂ gas. The crystals were kept under these conditions for an initial 16 h, followed by variable time intervals (Table 2). The total duration of the experiment (37–94 h) varied based on crystal thickness. FTIR analyses were performed after each step, to determine if hydrogen diffusion coupled to redox reaction (1) was arrested, and all hydrogen-associated defects in the clinopyroxene crystals were filled.

Previous studies used the experimental procedure above to rehydrate clinopyroxene (Bromiley and Keppler 2004; Skogby 2006; Sundvall et al. 2008; Weis et al. 2015), and show that under these specific conditions, hydrogen diffusion related to reaction (1) is several orders of magnitude

faster than vacancy diffusion. Therefore, at the given PT conditions and time intervals, resetting or creating new structural defects is not likely (Ingrin and Blanchard 2006; Ingrin and Skogby 2000).

FTIR spectroscopy

Polarised FTIR spectra were acquired on the oriented crystals in the 2000–15,000 cm^{-1} wavenumber interval along the three main refractive indices (α , β , and γ). The analyses were done with a Bruker Vertex 70 spectrometer equipped with a NIR source (halogen lamp) and a CaF_2 beamsplitter, coupled with a Hyperion 2000 microscope, with a ZnSe wiregrid polariser and an InSb detector. A total of 128 scans were acquired and averaged for both the background and the samples, with a 4 cm^{-1} resolution. The aperture was adjusted (100–200 μm) for masking, to avoid any cracks and inclusions. Crystal thickness varied between 85 and 950 μm , with most crystals having a thickness between 200 and 360 μm for both (100) and (010) orientations.

The spectra obtained were baseline corrected by a polynomial function and the characteristic OH peaks were fitted with the PeakFit software. The water content was calculated through a modified equation of the Beer-Lambert law: $c = A_{\text{to}}/(\epsilon \times t)$, where c is the water content in ppm by weight, A_{tot} is $A_{\alpha} + A_{\beta} + A_{\gamma}$ (the integrated absorbance measured parallel to the optical indicatrix directions) expressed in cm^{-2} , and t is the thickness in cm and ϵ is the specific absorption coefficient. In this study, we use the wavenumber-dependent calibration by Libowitzky and Rossman (1997).

Mössbauer spectroscopy

The oxidation states of iron (Fe^{2+} and Fe^{3+}) before and after experimental rehydration were obtained by Mössbauer spectroscopy. Several crystals from each sample were powdered (~1–3 mg) and mixed with thermoplastic resin and shaped under mild heat (~80 °C) into a cylindrical absorber (1x2 mm). The samples were then mounted on a strip of tape and analysed with a ^{57}Co point source (active diameter 0.5 mm), at room PT conditions, at a 90° incident angle to the γ rays. All spectra were calibrated against an α -Fe foil, folded and reduced from 1024 to 512 channels, and fitted with the MossA software. For fitting, two doublets were assigned for Fe^{2+} and one doublet for Fe^{3+} in the M1 and M2 octahedral positions. The percentage of each oxidation state of iron relative to the total iron content ($\pm 1\%$) was obtained from the areas of the doublets, assuming similar recoil-free fractions for Fe^{2+} and Fe^{3+} .

Magmatic water content calculation

The pre-eruptive magmatic water content of the host basaltic magma was calculated using the water contents measured

after H_2 -treatment and a water partition coefficient specific for Ca-rich clinopyroxene and silicate melts. The amount of hydrogen incorporated in the pyroxene structure is often correlated to the amount of tetrahedral aluminium. As such, the partition coefficient between each analysed crystal and its parental magma was calculated using the equation of O'Leary et al. (2010): $\ln D = -4.2 (\pm 0.2) + 6.5 (\pm 0.5)^{\text{VI}}[\text{Al}^{3+}] - 1.0 (\pm 0.2)[\text{Ca}^{2+}]$. Subsequently a pre-eruptive magmatic water content was calculated for each crystal and averaged per sample.

Thermobarometry

Crystallisation pressures and temperatures were determined for the investigated samples by using the measured clinopyroxene compositions, calculated magmatic water content, and whole-rock data from Bindeman et al. (2022). We applied the clinopyroxene-liquid barometer by Neave and Putirka (2017) coupled with the thermometer (equation 33) from Putirka (2008), both employing jadeite-diopside/hedenbergite exchange equilibria between clinopyroxene and the host magma. We used a double iteration method, based on equation (30) from Putirka (2008) and the pressure-independent thermometer from Putirka et al. (1996), for calibration. The Neave and Putirka (2017) barometer was proven to be reliable when calculating pressures up to 20 kbar for samples of basaltic composition (Nazzareni et al. 2020), improving on previous barometers (e.g., equation 30, Putirka (2008)). We tested for equilibrium on the basis of Fe-Mg partition coefficient between the clinopyroxene crystals and the host magma, and obtained $K_D(\text{Fe-Mg})^{\text{cpX-liq}}$ values in compliance with the 0.28 ± 0.08 required (Putirka 2008), and by comparing multiple “predicted” clinopyroxene components with those calculated (Geiger et al. 2018; Mollo et al. 2013).

Results

Major element mineral chemistry

The clinopyroxene major element compositions obtained by EMPA and the calculated cations per formula unit are listed in supplementary Table A1. All analysed clinopyroxene crystals are augites with relatively low (0.15–0.31 wt.%) TiO_2 content (Table A1 and Fig. 2). The compositions obtained fall in the same range as those obtained by Halldórsson et al. (2022), and are similar to clinopyroxene from other Icelandic eruptions (North Volcanic Zone, Hartley and Thordarson (2013); EVZ–East Volcanic Zone, Passmore (2009); South Volcanic Zone, Nikkola et al. (2019)). The Mg# values range between 0.86 and 0.89, with no significant variations recorded among different grains of the same sample. Similarly, no intra-crystalline heterogeneities were observed in

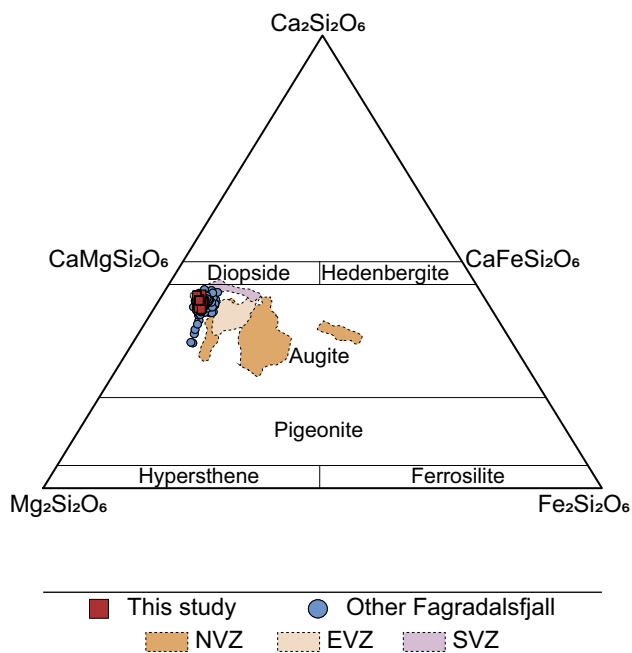


Fig. 2 Compositional classification of clinopyroxene (after Morimoto (1988)). The samples from this study are marked with red squares, and plot in the augite field. Other clinopyroxene compositions are marked with blue circles (Fagradalsfjall 2021 eruption, Halldórsson et al. (2022)); dark orange field (NVZ–North Volcanic Zone, Hartley and Thordarson (2013)); light orange field (EVZ–East Volcanic Zone, Passmore (2009)); purple field (SVZ South Volcanic Zone, Nikkola et al. (2019))

the BSE images, nor between the compositions measured in different spots per grain. The calculated $^{VI}Al/^{IV}Al$ ratio varies between 1.5 and 1.9 (1.7 ± 0.09 average value).

FTIR analysis and rehydration

All analysed crystals show typical absorption bands at 3640, 3520, and 3460 cm^{-1} in the IR spectra (Fig. 3), with the former most prominent when measured along the α and β directions, and the latter, around 3520 and 3460 cm^{-1} , most marked along the γ direction. This pleochroic behaviour, common in clinopyroxene, is due to the OH dipole being crystallographically oriented (Beran 1976; Skogby et al. 1990; Weis et al. 2015). The absence of a peak around 5200 cm^{-1} and of a broader band in the 3000–3700 cm^{-1} region indicates that the absorbing hydrogen configuration is OH, and there is no significant H_2O contribution from within the crystal or nanometre-sized fluid inclusions. Prior to H_2 heat treatment, the crystals show very weak absorptions and peaks, which increase significantly in all three directions after the treatment (Fig. 3). The most significant change in the absorption spectra is the height increase of the peak at 3640 cm^{-1} , with the peak positions

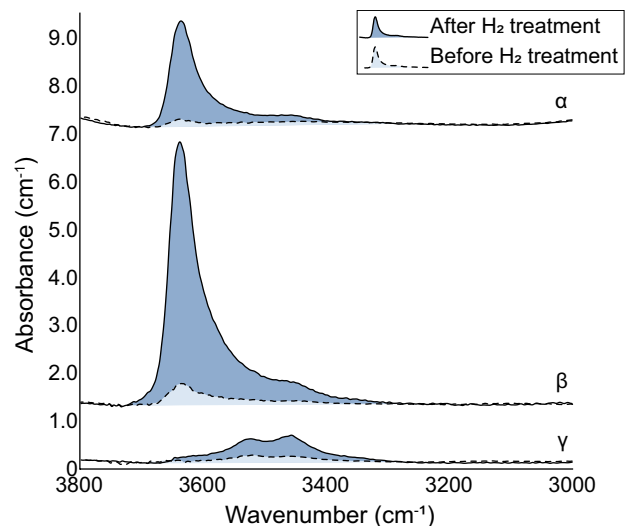


Fig. 3 Representative IR-spectra of clinopyroxene from the Geldingadalir 2021 eruption. The polarised spectra were measured parallel to the main refractive indices (α , β , γ) and show three main absorption bands at 3640, 3520, and 3460 cm^{-1} , which relate to different OH-dipole orientations (see text for details). The light blue area corresponds to water content measured on the untreated crystal, and the dark blue area corresponds to water content measured after H_2 -experiments were performed. The spectra shown were measured on sample Fagra1(1) and show a marked increase in peak intensity and thus in corresponding water content

remaining unchanged. The corresponding water content, calculated with the Libowitzky and Rossman (1997) wavenumber-dependent calibration, registers an equally significant increase (Table 2). The untreated crystals yield water contents of ~5–30 ppm, which increases to 110–175 ppm after hydrogen treatment. The water content shows minor variation among the crystals from the same sample, or among the different samples (Fig. 4), which may be accounted for by errors due to the peak fitting process.

Mössbauer analysis

The detailed parameters for Mössbauer spectroscopy are shown in Table 3 and representative spectra with doublets for Fe^{2+} and Fe^{3+} , measured on untreated and H_2 -treated samples, are shown in Fig. 5. The $\text{Fe}^{3+}/\text{Fe}_{\text{tot}}$ ratio of the untreated clinopyroxene crystals ranges between 12 and 13%, and upon H_2 heat treatment, all samples register a 30 to 45% reduction of Fe^{3+} (3.6–6.0% ΔFe^{3+} measured, Table 4).

Magmatic water contents

The average magmatic water content calculated using the water concentrations of experimentally rehydrated crystals

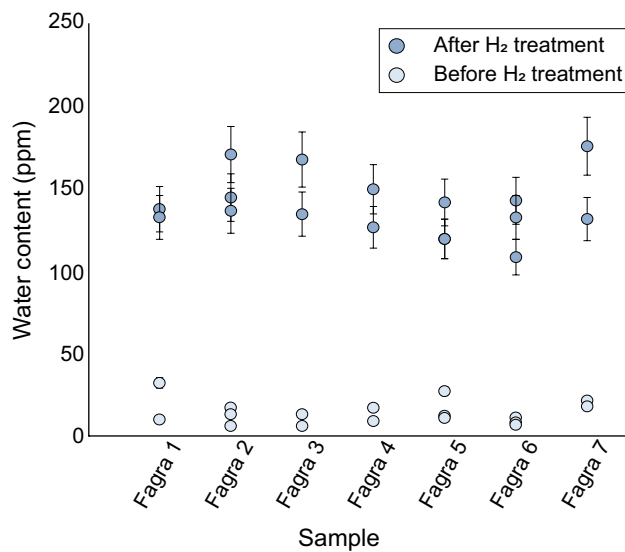


Fig. 4 Water content distribution among untreated and H₂-treated clinopyroxene crystals. The contents are based on FTIR measurements and show an increase between the untreated (light blue) and the H₂-treated (dark blue) crystals, with no significant variation within individual samples. The error bars correspond to $\pm 10\%$

and the partition coefficients from the equation of O'Leary et al. (2010) varies between 0.65 ± 0.06 and 0.86 ± 0.09 wt.% (Table 5). There is no detectable variation among the samples from different vents or eruption dates. All calculated magmatic water contents, before and after H₂ treatment, are summarised in Fig. 4.

Thermobarometry

Estimating the crystallisation pressures and temperatures is essential for calculating the depths at which magma was stored prior to eruption and for integrating our petrological and geochemical results within the active volcanic setting. Basing these estimates on pyroxene-liquid chemical exchange equilibria was experimentally proven to be a reliable method, as pyroxene crystallises early in mafic melts and its composition is very sensitive to pressure changes at magmatic temperatures (Neave and Putirka 2017; Putirka 2008). Of the clinopyroxene crystals analysed for major elements, 26 crystals were used for the P-T determinations and have partitioning coefficients ($K_D(\text{Fe-Mg})^{\text{cpx-liq}}$) with the associated melt ranging between 0.28 and 0.29 (Table 6).

Using the clinopyroxene-liquid barometer of Neave and Putirka (2017) combined with the thermometer of Putirka (2008) and the calculated magmatic water content, the investigated clinopyroxene yield pressures and temperatures ranging from 1.9 to 5.3 kbar and ~ 1210

to ~ 1255 °C. Assuming a rock column density of 3111 kg/m^3 (Tenzer 2013), these P-T conditions correspond to crystallisation depths between 6 and 16 km, pointing towards an average storage depth of 10 km.

Discussion

Clinopyroxene rehydration and associated processes

The water content before H₂ treatment varies among the investigated samples and among crystals from the same sample by a factor of 2 to 3 (Table 2), despite their relatively homogeneous major element composition. This variation is likely due to different degrees of pre- or syneruptive dehydration, controlled by grain size and local PT conditions or oxidising gradients within the host magma, and does not reflect variations of primary H₂O content in the parental liquids. After H₂ treatment, the water content is comparatively homogeneous in each sample (Fig. 4), roughly within the 10% error of FTIR analysis, showing that most crystals reached saturation within 37h of the experiment. For the rehydrated crystals, only minor variations are recorded among the different samples (Table 2), which are almost within the analytical error. However, there is no correlation between water content and sampling date or location.

For the untreated crystals, we propose that hydrogen loss was driven by outward diffusion, which at magmatic temperatures (>800 °C) can occur over several millimetres in a few hours (Woods et al. 2000). If dehydration took place during the eruption, diffusion profiles showing outward decreasing water contents could be quenched in the crystals; however, no such profiles were recorded in our samples. This might be either due to the crystal rims being partially removed during polishing, or they might be undetected at the level of the spatial resolution of the FTIR analyses. Alternatively, in a slow cooling magma, no such profiles would be expected. Hydrogen solubility and diffusion are also controlled by fluid pressure and redox conditions. Upon magma ascent, volatiles are exsolved and lost, and fluid pressure in the magma decreases. The clinopyroxene crystals equilibrating with the progressively degassing magma are expected to lose their hydrogen content partly or totally, following the redox reaction (1). Within the conduit system, the redox state of the magma may be influenced by reactions coupled with SO₂ exsolution, making it progressively more reduced (Métrich et al. 2009; Moussallam et al. 2014). However, given the low abundance of pyroxene phenocrysts within the sampled lavas (0.005–0.015%), with concentrations of ~ 0.013 wt.% H₂O/crystal, most of the water in the system would have remained in the melt prior to eruption. Moreover, the SO₂/H₂O emission ratio measured at the vents is of 1:10

Table 3 Mössbauer spectroscopy results (all analyses were done with point source)

Sample	Multiplet	Initial				After H ₂ treatment				ΔFe^{3+} (%)
		int (%)	fwhm (mm/s)	cs (mm/s)	qs (mm/s)	int (%)	fwhm (mm/s)	cs (mm/s)	qs (mm/s)	
Fagra 1										
Fe ²⁺	Doublet 1	69.5	0.44	1.15	1.96	61.2	0.42	1.14	1.93	36
	Doublet 2	18.9	0.44	1.17	2.44	31.3	0.45	1.14	2.34	
Fe ³⁺	Doublet 1	11.6	0.59	0.44	0.56	7.47	0.51	0.50	0.50	
Fagra 2										
Fe ²⁺	Doublet 1	61.7	0.42	1.15	1.93	77.6	0.46	1.14	1.97	31
	Doublet 2	25.0	0.44	1.16	2.40	13.3	0.39	1.11	2.52	
Fe ³⁺	Doublet 1	13.3	0.59	0.42	0.64	9.10	0.57	0.45	0.50	
Fagra 3										
Fe ²⁺	Doublet 1	66.6	0.44	1.14	1.95	82.1	0.48	1.14	1.99	47
	Doublet 2	21.8	0.45	1.15	2.46	11.8	0.35	1.12	2.55	
Fe ³⁺	Doublet 1	11.7	0.65	0.43	0.50	6.1	0.42	0.60	0.45	
Fagra 4										
Fe ²⁺	Doublet 1	47.4	0.43	1.15	1.89	82.6	0.48	1.15	1.98	39
	Doublet 2	39.2	0.55	1.15	2.35	9.2	0.31	1.15	2.56	
Fe ³⁺	Doublet 1	13.4	0.54	0.42	0.70	8.2	0.60	0.42	0.60	
Fagra 5										
Fe ²⁺	Doublet 1	59.0	0.43	1.15	1.90	75.7	0.48	1.15	1.96	36
	Doublet 2	24.6	0.42	1.17	2.46	12.8	0.38	1.15	2.50	
Fe ³⁺	Doublet 1	16.4	0.60	0.43	0.60	10.4	0.60	0.43	0.77	
Fagra 6										
Fe ²⁺	Doublet 1	59.8	0.42	1.14	1.96	72.3	0.48	1.15	1.96	25
	Doublet 2	25.7	0.43	1.16	2.60	16.9	0.39	1.16	2.49	
Fe ³⁺	Doublet 1	14.5	0.60	0.43	0.55	10.9	0.60	0.42	0.55	
Fagra 7										
Fe ²⁺	Doublet 1	58.7	0.44	1.14	1.95	65.1	0.44	1.15	1.90	30
	Doublet 2	29.0	0.44	1.16	2.40	26.3	0.43	1.14	2.40	
Fe ³⁺	Doublet 1	12.1	0.63	0.43	0.60	8.5	0.51	0.40	0.68	

int, intensity in percentage $\text{Fe}^{m+}/\text{Fe}_{\text{total}}$; *fwhm*, full width at half maximum (including source width); *cs*, centroid shift; *qs*, quadrupole splitting

(Halldórsson et al. 2022). Sulphur exsolution would have therefore had a negligible effect on the melt/clinopyroxene water exchange. Additional late-stage degassing may occur upon exposure to the oxidising atmosphere during eruption. It is likely that degassing and oxidising processes will affect the magma unevenly, leading to local gradients and for some clinopyroxene crystals to lose more hydrogen than others. Another factor that may influence the amount of hydrogen lost through outward diffusion is the crystal size. Given that recent studies show that the 2021 eruption at Geldingadalir was fed directly from a near-Moho magma reservoir (Bindeman et al. 2022; Halldórsson et al. 2022) with no significant shallow crustal stalling, we consider dehydration within the conduits, i.e. during magma ascent, as most probable to explain the observed variations, but cannot fully exclude an influence from local heterogeneities in the host magma, or from oxidising processes upon eruption.

Mössbauer spectroscopy was used on non-treated pyroxene crystals, and crystals that underwent similar H₂ experimental treatment, to verify the role of redox reaction (1) during hydrogen loss and gain. The results obtained demonstrate a reduction of $\text{Fe}^{3+}/\text{Fe}_{\text{total}}$ by 25–47% after thermal annealing (Table 3) with a median value at 36%. The change in the Fe^{3+} atoms per formula unit (pfu) expected for a 1:1 proportion with the hydrogen uptake is significantly lower (Table 4). The ΔFe^{3+} pfu calculated based on measured OH content increase during rehydration, following the redox reaction (1), varies from 1.1 ± 0.1 to $1.7 \pm 0.1\%$, whereas the measured ΔFe^{3+} pfu ranges from 3.6 ± 0.2 to $6.0 \pm 0.3\%$. This difference could be due to the combined analytical error of Mössbauer and FTIR analyses or caused by the small variations in major element composition and water content among different crystals. The $\text{Fe}^{3+}/\text{Fe}_{\text{total}}$ ratios were measured on several powdered crystals, whereas the calculated Fe^{3+} pfu and water content were determined for individual crystals.

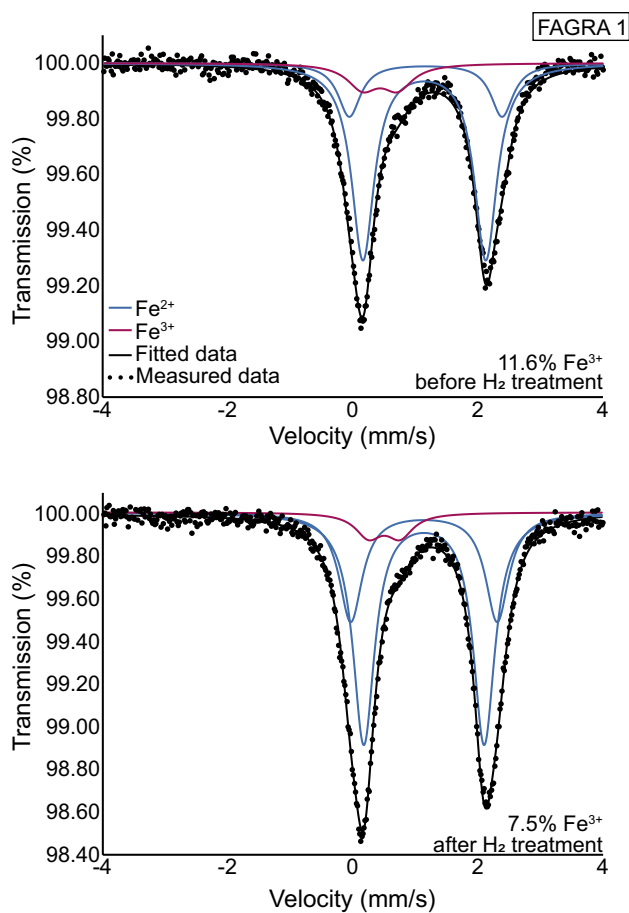


Fig. 5 Representative Mössbauer spectra for untreated and H₂-treated clinopyroxene. The spectra show typical Fe²⁺ (blue) and Fe³⁺ (red) doublets, used to estimate the ratio of the two iron oxidation states. The spectra shown were measured on clinopyroxene from sample Fagra1 and show a strong decrease in the Fe³⁺ content after H₂-treatment, as expected (see text for details)

Table 4 Changes in Fe³⁺/Fe_{total} after H₂-treatment

Sample	ΔOH (pfu)*	Fe _{total} (pfu)	ΔFe ³⁺ (pfu) expected (%)**	ΔFe ³⁺ measured (%)***
Fagra 1	0.0015 ± 0.0002	0.1429	1.2 ± 0.05	4.1 ± 0.2
Fagra 2	0.0017 ± 0.0002	0.1460	1.3 ± 0.12	4.2 ± 0.2
Fagra 3	0.0016 ± 0.0000	0.1381	1.2 ± 0.09	5.5 ± 0.2
Fagra 4	-	-	-	5.2 ± 0.2
Fagra 5	0.0014 ± 0.0000	0.1424	1.1 ± 0.09	6.0 ± 0.3
Fagra 6	0.0015 ± 0.0002	0.1251	1.3 ± 0.07	3.6 ± 0.3
Fagra 7	0.0017 ± 0.0004	0.1306	1.7 ± 0.06	3.6 ± 0.2

*Change in water content per formula unit, after H₂ experimental treatment

**Expected change in Fe³⁺/Fe_{total} correlated to OH incorporation

***Change in Fe³⁺/Fe_{total} measured by Mössbauer spectroscopy

Similar deviations from the values expected for a 1:1 exchange following the redox reaction (1) were previously reported by Bromiley and Keppler (2004); Sundvall et al. (2008); and Weis et al. (2015).

Although there is no significant variation in the total Fe content of the different pyroxenes, the change in the amount of Fe³⁺ after hydrogen treatment is not constant (Table 3) and could explain the small water content variations post rehydration (e.g. Fagra 3: 47% ΔFe³⁺, up to 167 ppm wt. H₂O). Additionally, other mechanisms could contribute to hydrogen incorporation and an increase in water solubility in clinopyroxene with increasing ^{IV}Al³⁺ was previously noted by Hauri et al. (2006); Skogby (2006); and Weis et al. (2015).

Calculated PT conditions and magmatic water contents

The calculated crystallisation pressures and temperatures (1.9–5.3 kbar, ~1210–1255) for the studied clinopyroxene overlap with previous determinations for the 2021 Geldingadalir eruption (Halldórsson et al. 2022), and similarly, the estimated crystallisation depths (10 km average) are in agreement with the current models for magma storage beneath Fagradalsfjall (Fig. 6; Bindeman et al. (2022); Halldórsson et al. (2022)). These models imply a main near-Moho magma reservoir, located between 15 and 20 km depth, that was fed by various mantle sources. Within this contextual framework, we estimate the final equilibration of the clinopyroxene crystals with the host magma, as well as the formation of hydrogen-associated structural defects, to have taken place at the upper limit of the magma storage system and within the lower part of the magma conduit (Fig. 7a).

The average magmatic water contents from this study based on the dehydrated (non-treated) clinopyroxene (0.04–0.13 wt.% H₂O) are in agreement with those reported in glass shards by Bindeman et al. (2022) (0.00–0.22 wt.% H₂O) for the Geldingadalir 2021 eruption (Fig. 8). The latter, which underwent total or partial degassing during rapid lava cooling, register δD values (−69.2 to −109.7‰) consistent with both Rayleigh- and Batch-type fractionation during degassing (Bindeman et al. 2022) and indicate that the clinopyroxene crystals underwent similar processes. For Geldingadalir clinopyroxene, between 74 and 94% of the initial magmatic water content is estimated to have been lost during dehydration. Conversely, the contents we report here for the Geldingadalir magmas based on the rehydrated (H₂-treated) clinopyroxene (0.65–0.86 wt.% H₂O) overlap with the upper range of previous estimates for Icelandic subglacial volcanoes (0.10–1.02 wt.% H₂O, Nichols et al. (2002)) and with the lower range of water estimates for ocean island basalts generally (Dixon et al. 1997; Weis et al. 2015). These water

Table 5 Magmatic water content inferred from clinopyroxene

Sample	H ₂ O _{cpx} (ppm)*	D _(cpx/melt)	lnD _(cpx/melt)	^{VI} Al ³⁺	Ca ²⁺	H ₂ O _{melt} (wt.%)	Average H ₂ O _{melt} (wt.%)
Fagra 1 (1)	137	0.017	-4.094	0.137	0.786	0.8	0.82
Fagra 1 (2)	132	0.016	-4.138	0.130	0.781	0.8	
Fagra 2 (1)	144	0.017	-4.053	0.144	0.786	0.8	0.84
Fagra 2 (2)	136	0.016	-4.120	0.130	0.767	0.8	
Fagra 2 (3)	170	0.020	-3.919	0.163	0.779	0.9	
Fagra 3 (1)	134	0.018	-4.042	0.145	0.785	0.8	0.86
Fagra 3 (2)	167	0.018	-4.042	0.145	0.785	1.0	
Fagra 4 (1)	126	0.018	-4.042	0.145	0.785	0.7	0.78
Fagra 4 (2)	149	0.018	-4.042	0.145	0.785	0.8	
Fagra 5 (1)	119	0.017	-4.067	0.139	0.768	0.7	0.69
Fagra 5 (2)	119	0.021	-3.855	0.175	0.792	0.6	
Fagra 5 (3)	141	0.017	-4.067	0.138	0.767	0.8	
Fagra 6 (1)	132	0.019	-3.964	0.159	0.797	0.7	0.65
Fagra 6 (2)	142	0.019	-3.967	0.156	0.784	0.8	
Fagra 6 (3)	108	0.021	-3.854	0.176	0.797	0.5	
Fagra 7 (1)	175	0.019	-3.962	0.157	0.780	0.9	0.80
Fagra 7 (2)	131	0.019	-3.962	0.157	0.780	0.7	

*Water content after H₂-treatment**Table 6** Thermobarometry results

Sample	T (°C) (Putirka 2008)	Pressure* (kbar)	Depth** (km)	K _D (Fe-Mg) ^{cpx-liq}
Fagra 1 (1)_1	1228	3.09	10	0.29
Fagra 1 (1)_2	1229	3.12	10	0.29
Fagra 1 (2)_1	1220	2.29	7	0.29
Fagra 1 (2)_2	1220	2.07	6	0.29
Fagra 2 (1)_1	1219	2.53	8	0.29
Fagra 2 (1)_2	1221	2.56	8	0.29
Fagra 2 (2)_1	1236	3.81	12	0.29
Fagra 2 (2)_2	1236	3.78	12	0.29
Fagra 2 (3)_1	1232	3.62	11	0.29
Fagra 2 (3)_2	1237	4.00	12	0.29
Fagra 5 (1)_1	1233	3.83	12	0.29
Fagra 5 (1)_2	1236	3.84	12	0.29
Fagra 5 (2)_1	1246	5.26	16	0.29
Fagra 5 (2)_2	1238	4.66	15	0.29
Fagra 5 (3)_1	1254	5.23	16	0.29
Fagra 5 (3)_2	1240	4.75	15	0.29
Fagra 6 (1)_1	1238	4.16	13	0.29
Fagra 6 (1)_2	1209	1.93	6	0.28
Fagra 6 (2)_1	1239	4.16	13	0.29
Fagra 6 (2)_2	1223	2.87	9	0.29
Fagra 6 (3)_1	1246	5.22	16	0.29
Fagra 6 (3)_2	1236	4.22	13	0.29
Fagra 7 (2)_1	1230	3.43	11	0.29
Fagra 7 (2)_2	1230	3.37	10	0.29

*Calculated based on Neave and Putirka, 2017

**Estimated assuming a crusta-mantle average density of 3111 kg/m³ (Tenzer, 2013)

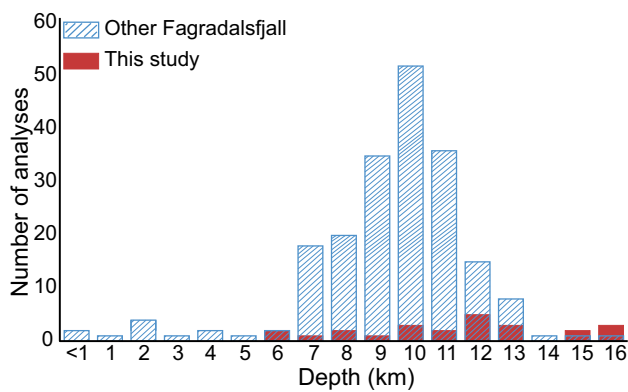


Fig. 6 Depth distribution for hydrogen incorporation in clinopyroxene. The calculated depths for crystallisation of clinopyroxene, and thus for hydrogen incorporation in crystal structural defects, range between 6 and 16 km for the studied samples (in red). Our barometric determinations overlap with the calculated depths for clinopyroxene from Halldórsson et al. (2022), shown for comparison (hashed blue)

contents are higher than average Mid-Atlantic and Reykjanes Ridge basalts (Bindeman et al. 2022; Michael and Schilling 1989; Nichols et al. 2002; Poreda et al. 1986) and likely reflect the variably water-enriched OIB-type magma compositions that fed the reservoir beneath Fagradalsfjall

(Bindeman et al. 2022; Halldórsson et al. 2022). This is in agreement with observations by Nichols et al. (2002), according to which the highest water contents along the Reykjanes Ridge (~0.4–1.1 wt.% H₂O), including the range we obtain for Geldingadalir magma (0.65–0.86 wt.% H₂O), are found in samples collected close (±200 km) to the plume centre. Since there was no prolonged ponding and equilibration of the magma at shallow crustal levels (Bindeman et al. 2022; Halldórsson et al. 2022) and given the estimated depth of the studied pyroxene (6–16 km), no resetting of structural defects is thought to have occurred post-crystal-magma equilibration. As such, the calculated magmatic water contents inferred from the H₂-treated crystals likely reflects the initial water content of the magma residing beneath Geldingadalir during the 2021 eruption. According to the evolution of the magmatic system with time (Bindeman et al. 2022; Halldórsson et al. 2022), the lava extruded at the start of the eruption, in March 2021, was mostly derived from a relatively depleted mantle source, and it rapidly became more enriched, with increasing contributions from a more enriched mantle source. In consequence, the calculated magmatic water contents for the April 2021 lava samples may offer insight into the water content of Icelandic plume magmas, at least in this region of the plume system.

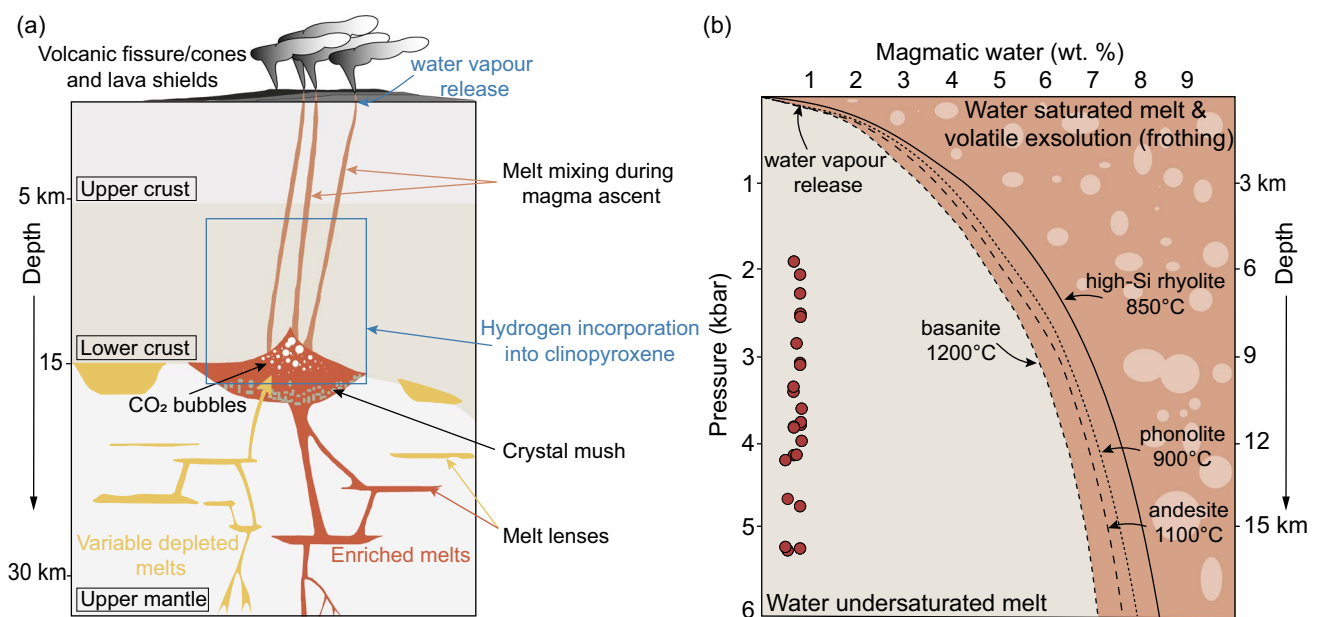


Fig. 7 a Conceptual model of melt generation, storage, and ascent beneath Geldingadalir. Magma is stored in the lower crust, near the Moho discontinuity, and is fed by various melts from depleted (yellow) and enriched (red) parts of the upper mantle. Prior to the eruption, hydrogen is incorporated during clinopyroxene crystallisation into structural defects, at ca 16 to 6 km depth (blue box), with an average estimated crystallisation depth of ca. 10 km and from a parental liquid containing 1.12 ± 0.36 wt.% H₂O. Hydrogen loss

likely occurred during magma ascent and post-eruption degassing of the lava (see text for details). Sketch after Bindeman et al. (2022); Halldórsson et al. (2022). **b** Comparison of H₂O solubility models for various magma compositions. Variation in water solubility with pressure for different compositions is represented with solid and dashed lines (after Moore et al. (1998)), and the studied samples from Geldingadalir are marked with red symbols

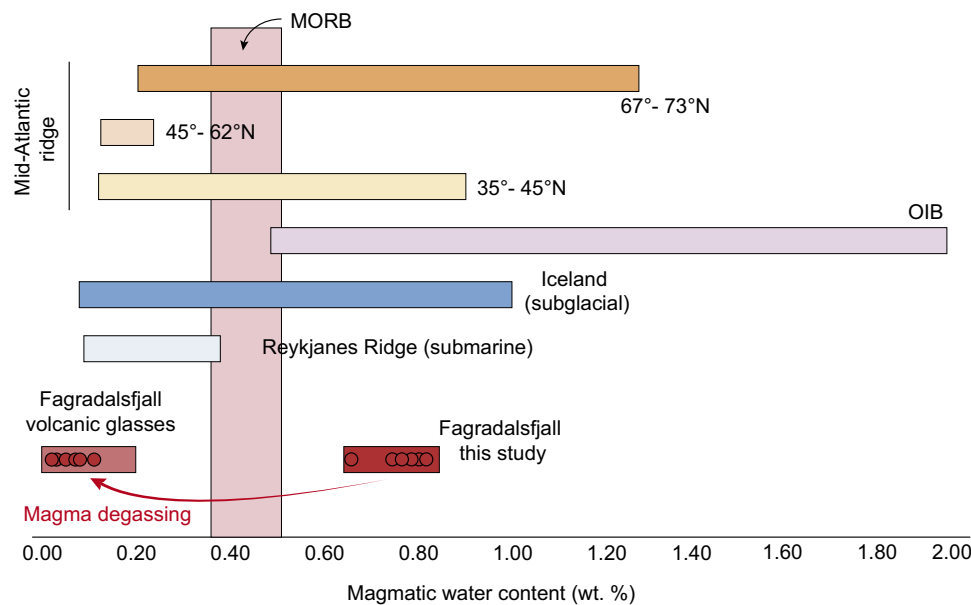


Fig. 8 Comparison of magmatic water contents of the Geldingadalir 2021 eruption and other Icelandic and Mid-Ocean Ridge Basalt (MORB) compositions. Water contents from this study (red circles and dark red bar) are based on rehydrated clinopyroxene crystals. Previous values for Geldingadalir eruption based on volcanic glass measurements and standard MORB (UOB reference material)

are from Bindeman et al. (2022); estimates for submarine Reykjanes ridge and subglacial Icelandic magmas are from Nichols et al. (2002) and Poreda et al. (1986); estimates for Ocean island basalts (OIB) are from Dixon et al. (1997) and Weis et al. (2015); estimates for Mid-Atlantic ridge basalts are from Michael and Schilling (1989)

Magma degassing and volcanological implications

With decreasing total fluid pressure ($PCO_2 + PH_2O$), the solubility of volatiles (i.e. CO_2 , H_2O , SO_2) in magma decreases (Burton et al. 2007; Holloway and Blank 1994; Moore et al. 1998), and as the magma becomes saturated and these volatile species are exsolved, gas bubbles begin to form and accumulate (Fig. 7b). In the case of the Geldingadalir 2021 eruption, following pre-eruptive deformation patterns and inferred volume change, it is likely that a volatile mixture of $\geq 70\%$ CO_2 exsolved from the initial magma and ascended as an immiscible supercritical fluid before the onset of the eruption (Flóvenz et al. 2022). This conceptual model indicates an earlier and deeper CO_2 exsolution resulting in high CO_2 emissions, as a background for shallow H_2O and SO_2 exsolution during the eruption (Sigmundsson et al. 2020). This is an agreement with multispectral data for surface gas emissions and groundmass glass compositions (Halldórsson et al. 2022). Alternatively, assuming closed-system degassing and by coupling the measured surface gas emissions and melt inclusions volatile composition as proxy for the parental magma, the minimum CO_2 saturation pressure is estimated at 5.1 ± 1.5 kbar (≥ 18 km depth) arguably driving magma extraction from the near-Moho reservoir (Halldórsson et al. 2022). Since the untreated clinopyroxene crystals

analysed in this study yield similar magmatic water contents to those reported by Bindeman et al. (2022) from volcanic glasses, it is likely that they witnessed similar water vapour exsolution processes in the magma, prior to and during the eruption. Given the solubility of water in basaltic magmas at different pressures (Fig 7b), and the relatively low water content in the dehydrated Geldingadalir samples (0.04–0.13 wt.% H_2O), we constrain the depth for water exsolution to the uppermost few hundreds to tens of metres below the surface.

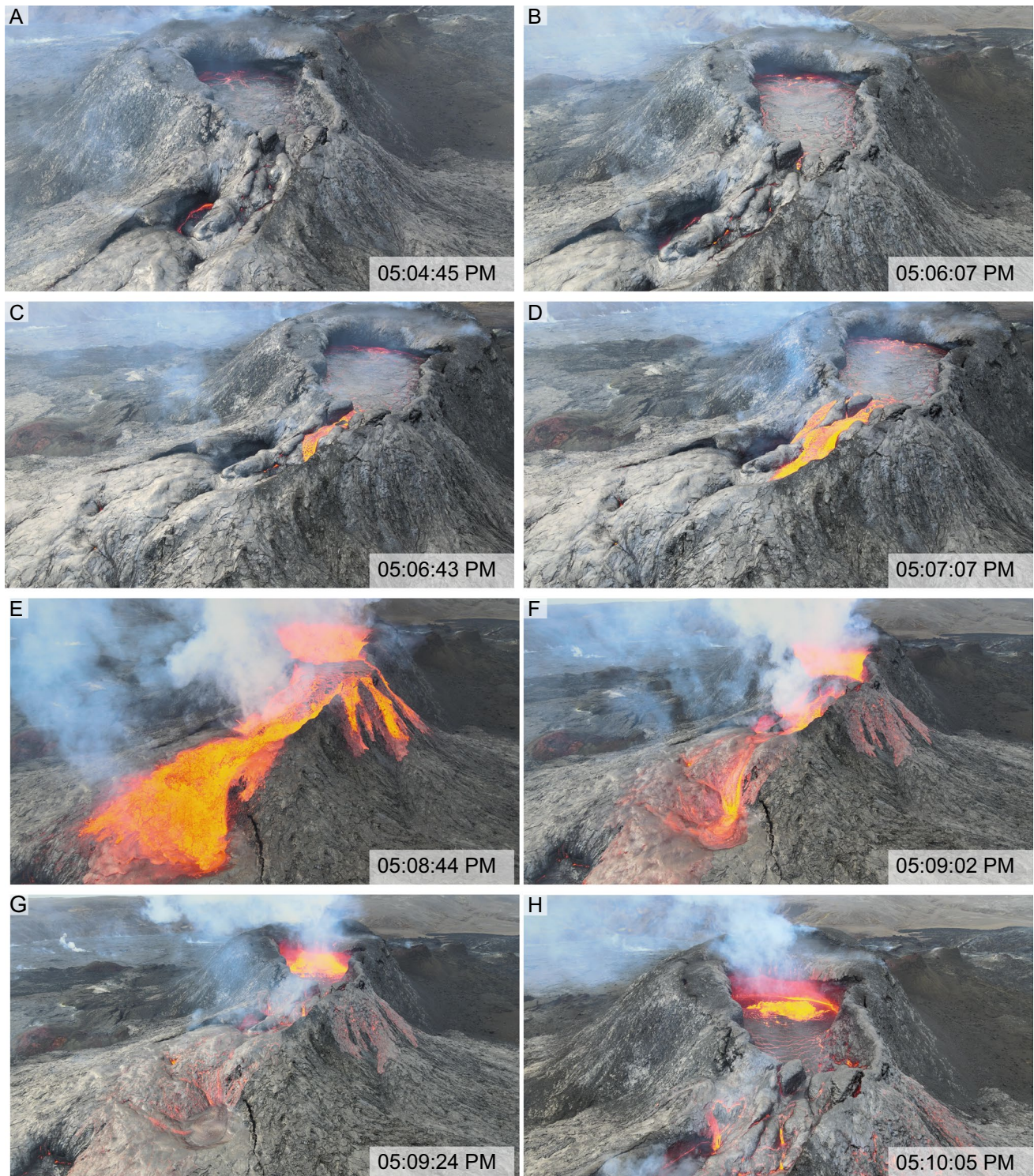
The contribution of multiple enriched mantle source components, with variable compositions and densities, to the 2021 eruption (Bindeman et al. 2022; Halldórsson et al. 2022), are expected to have been a source for variable, generally elevated volatiles (e.g. CO_2 , SO_2 , H_2O), compared to MORB-type magma compositions. These volatiles would have exsolved from the progressively over-saturated magma during storage and ascent, leading to nucleation of bubbles once the solubility curve for the various gas species is overstepped (Fig 7b). The vesicular, ascending magma would have been exposed to further decompression leading to a permeable gas flow that would allow additional volatiles to be released in the upper conduit system and for the gas phase to overtake the magma in the conduit (Burton et al. 2007; Polacci et al. 2015). At Geldingadalir, this would be



Acquisition date: June 8th 2021, time stamps in UCT

Fig. 9 Aerial images of the main active crater at Geldingadalir. Extracted frames from video recording of the erupting crater on the 8th of June 2021. The lava flow was roughly towards the south, and the images were acquired from south of the crater, at ~50m altitude,

with the camera oriented northward, facing the main discharge direction. On the day of acquisition, the eruption was stable, with pulsating flows at regular intervals of 8–10 min on average.

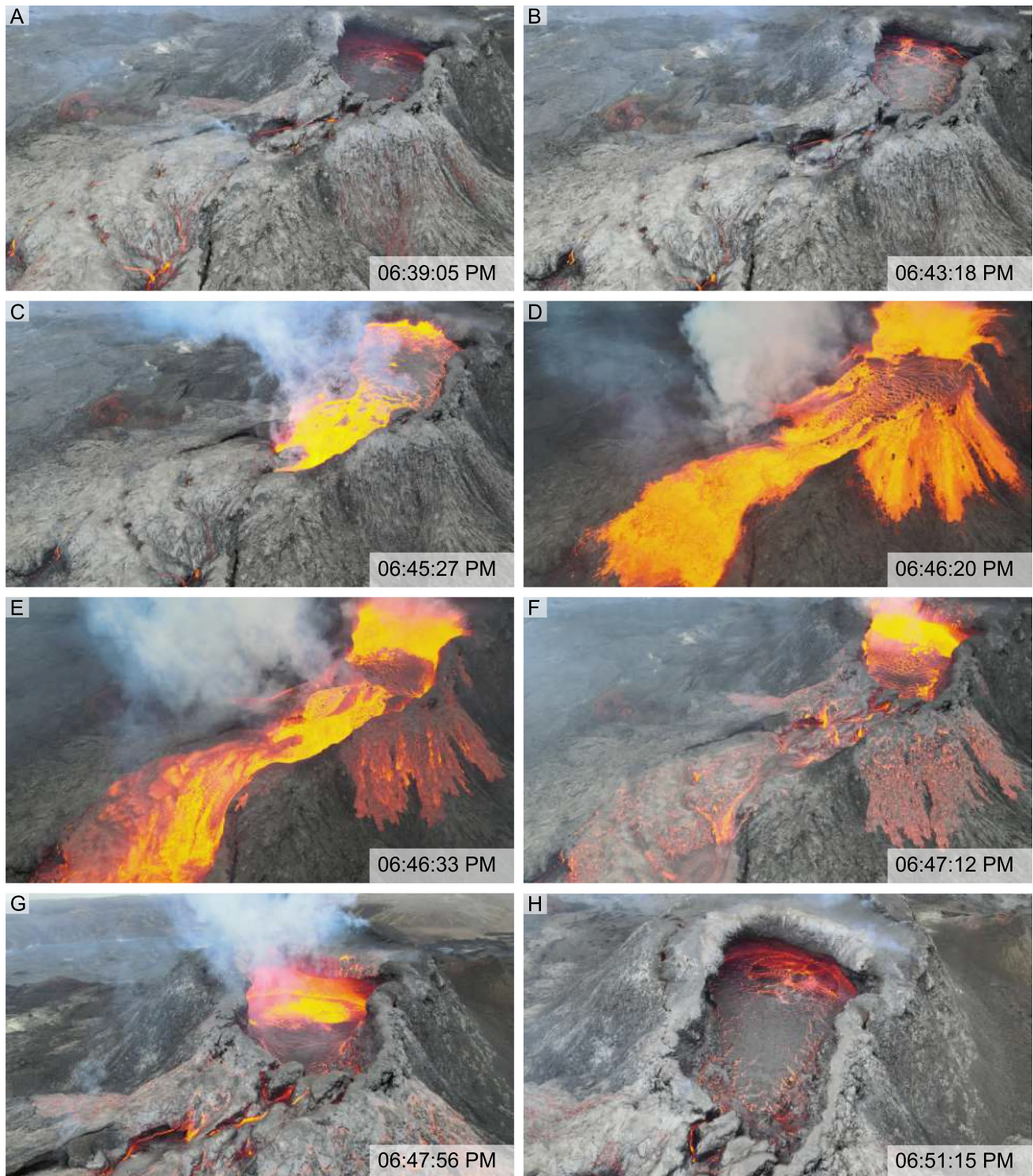


Acquisition date: June 8th 2021, time stamps in UCT

Fig. 9 (continued)

especially important, as the low water content would hinder saturation and exsolution in the deeper part of the system. Given the solubility of water in basaltic melts (Holloway and

Blank 1994; Moore et al. 1998), the Geldingadalir magmas filling the upper conduits and vents would thus be prone to shallow bubble growth and coalescence, as they would only



Acquisition date: June 8th 2021, time stamps in UCT

Fig. 9 (continued)

become over-saturated in water vapour at very high levels in the plumbing system (Figs. 7 and 9). As saturation and water exsolution would be restricted only to the top few hundred

to tens of metres below the surface, it would have a direct effect on the volume of gas-charged, bubbly magma that filled the upper conduit and lava pond during the eruption.

The rhythmic periods of “building-up and overflow” of the vent are best explained by this model of vesicle growth of the magma entering the shallow conduits and bottom of the lava pond, triggering a sudden onset of water vapour released close to the surface, causing rapid volume increase and overflow (Polacci et al. 2015). Once the maximum overflow is reached, the intensity is expected to decrease, and as the magma within the system is drained and the upper conduit is recharged with new magma from below. The new magma would then experience similar decompression in the top few hundred to tens of metres below the surface, followed by intense vesiculation as water vapour is exsolved, and in consequence, the magma-gas mixture volume would increase again leading to a new overflow. Although episodic release of SO₂ and CO₂ gas was recorded at the vents during the eruption period, the frequency was at significantly wider time intervals (the order of days) and is likely unrelated to the observed rhythmic overflows of the vent 5 of the 2021 Geldingadalir eruption, at 10- to 20-min intervals (Fig. 9). A similar model is proposed by Eibl et al. (2022) based on seismic data and direct observations of the 2021 Geldingadalir eruption. Magma rises, driven by vesiculation and degassing, progressively intensifying until it reaches maximum fountaining (> 300m height) and lava outpouring. Once the peak has been reached, the intensity gradually decreases and the outgassed lava retreats into the shallow conduit system, leaving the crater in a state of rest, until vesiculation and degassing reach the critical point after-which a new episode of magma expansion and overflow begins (Eibl et al. 2022). Within this model and based on the estimated primary water content (up to 0.9 wt.%) and rate of degassing from our studied samples (74–94%), intense dehydration likely took place in the top 50 m of the conduit system.

Conclusions

Parental magmatic water contents can be derived from clinopyroxene crystals after experimental H₂-treatment despite magma degassing during eruption. The average water contents of parental magmas supplying the early phase (April 2 to 10 2021) of the Fagradalsfjall Fires eruption are between 0.65 and 0.86 wt.% H₂O, in agreement with previous estimates for Icelandic subglacial volcanoes (Nichols et al. 2002). Furthermore, they are considerably higher than those obtained for Reykjanes Ridge or mid-Atlantic ridge basalts, but within the range obtained for Ocean Island basalts. The determined H₂O contents therefore probably reflect primary water contents of enriched plume melts that fed the 2021 eruption.

Based on the magmatic water content calculated from rehydrated clinopyroxene (0.65–0.86 wt.% H₂O) and established

basalt water solubility curves (Moore et al. 1998), we infer that water degassing of ascending magmas was restricted to the top few hundred metres below the surface. We therefore propose that repeated water vapour exsolution within the upper conduit system, that added a substantial gas volume to the deep-sourced magmatic CO₂ flux, was likely the cause for the rhythmic overflow observed in summer 2021.

Supplementary Information The online version contains supplementary material available at <https://doi.org/10.1007/s00445-023-01641-4>.

Acknowledgements The authors are grateful to Dr Nicole Métrich for their editorial handling and two anonymous reviewers for their helpful comments; to Edgar Zorn and Alina Shevchenko for collecting the samples for this study; and to Marius Isken and Erica De Paolo for assisting with drone image acquisition. We further acknowledge discussion with Ilya Bindeman, Arman Höskulsson, Thomas Walter, and William Moreland, and technical support from Hiltrud Müller-Sigmund at the EMPA in Freiburg.

Funding Open access funding provided by Swedish Museum of Natural History. Financial support from the Swedish Research Council (grant number 2018-05102 to IBR, HS; grant numbers 2020-03789 to VRT and 2018-04933 to FMD) and from the Riksmusei vänner (IBR) is gratefully acknowledged.

Declarations

Conflict of interest The authors declare no competing interests.

Open Access This article is licensed under a Creative Commons Attribution 4.0 International License, which permits use, sharing, adaptation, distribution and reproduction in any medium or format, as long as you give appropriate credit to the original author(s) and the source, provide a link to the Creative Commons licence, and indicate if changes were made. The images or other third party material in this article are included in the article's Creative Commons licence, unless indicated otherwise in a credit line to the material. If material is not included in the article's Creative Commons licence and your intended use is not permitted by statutory regulation or exceeds the permitted use, you will need to obtain permission directly from the copyright holder. To view a copy of this licence, visit <http://creativecommons.org/licenses/by/4.0/>.

References

- Aubaud C, Hauri EH, Hirschmann MM (2004) Hydrogen partition coefficients between nominally anhydrous minerals and basaltic melts. *Geophys Res Lett* 31(L20611)
- Barsotti S, Parks M, Pfeffer MA, Óladóttir B, Barnie T, Titos M, Jónsdóttir K, Pedersen GBM, Hjartardóttir ÁR, Stefansdóttir G, Johannsson T, Arason Þ, Gudmundsson M, Oddsson B, Prastarson R, Ófeigsson B, Vogfjörð K, Geirsson H, Hjörvar T et al (2023) The eruption in Fagradalsfjall (2021, Iceland): how the operational monitoring and the volcanic hazard assessment contributed to its safe access. *Nat Hazards*
- Beran A (1976) Messung des Ultrarot-Pleochroismus von Mineralen. XIV. Der Pleochroismus des OH-Streckfrequenz in Diopsid. *Tschermaks Mineral Petrogr Mitt* 23:79–85
- Bindeman IN, Deegan FM, Troll VR, Thordarson T, Höskulsson A, Moreland WM, Zorn EU, Shevchenko AV, Walter TR (2022)

- Diverse mantle components with invariant oxygen isotopes in the 2021 Fagradalsfjall eruption, Iceland. *Nat Comm* 13:3737
- Bromiley GD, Keppler H (2004) An experimental investigation of hydroxyl solubility in jadeite and Na-rich clinopyroxenes. *Contrib Mineral Petrol* 147(2):189–200
- Burton MR, Mader HM, Polacci M (2007) The role of gas percolation in quiescent degassing of persistently active basaltic volcanoes. *Earth Planet Sci Lett* 264:46–60
- Cabral RA, Jackson MG, Koga KT, Rose-Koga EF, Hauri EH, Whitehouse MJ, Price AA, Day JMD, Shimizu N, Kelley KA (2014) Volatile cycling of H₂O, CO₂, F, and Cl in the HIU mantle: a new window provided by melt inclusions from oceanic hot spot lavas at Mangaia, Cook Islands. *Geochem Geophys Geosyst* 15:4445–4467
- Cashman KV (2004) Volatile controls on magma ascent and eruption. In: Sparks RSJ, Hawkesworth CJ (eds) *The State of the Planet: Frontiers and Challenges in Geophysics*. American Geophysical Union
- Cassidy M, Ebmeier SK, Helo C, Watt SFL, Caudron C, Odell A, Spaans K, Kristianto P, Triastuty H, Gunawan H, Castro JM (2019) Explosive eruptions with little warning: experimental petrology and volcano monitoring observations from the 2014 eruption of Kelud, Indonesia. *Geochem Geophys Geosyst* 20(8):4218–4247
- Cherniak DJ, Dimanov A (2010) Diffusion in pyroxene, mica and amphibole. *Rev Mineral Geochem* 72(1):641–690
- Dixon JE, Clague DA, Wallace P, Poreda R (1997) Volatiles in alkalic basalts from the North Arch Volcanic Field, Hawaii: extensive degassing of deep submarine-erupted alkalic series lavas. *J Petrol* 38(7):911–939
- Edmonds M, Wallace P (2017) Volatiles and exsolved vapor in volcanic systems. *Elements* 13(1):29–34
- Eibl EPS, Thordarson T, Höskuldsson Á, Gudnason EÁ, Dietrich T, Hersir GP, Ágústsdóttir T (2022) Evolving shallow conduit revealed by tremor and vent activity observations during episodic lava fountaining of the 2021 Fagradalsfjall Eruption, Iceland. *Bull Volcanol* 85
- Einarsson P (2008) Plate boundaries, rifts and transforms in Iceland. *Jökull* 58:35–58
- Ferguson DJ, Gonnermann HM, Ruprecht P, Plank T, Hauri EH, Houghton BF, Swanson DA (2016) Magma decompression rates during explosive eruptions of Kīlauea volcano, Hawaii, recorded by melt embayments. *Bull Volcanol* 78(71)
- Flóvenz ÓG, Wang R, Hersh GP, Dahm T, Hainzl S, Vassileva M, Drouin V, Heimann S, Isken MP, Gudnason EÁ, Ágústsson K, Ágústsdóttir T, Horálek J, Motagh M, Walter TR, Rivalta E, Jousset P, Krawczyk CM, Milkereit C (2022) Cyclical geothermal unrest as a precursor to Iceland's 2021 Fagradalsfjall eruption. *Nat Geosci* 15:397–404
- Geiger H, Troll VR, Jolis EM, Deegan FM, Harris C, Hilton DR, Freda C (2018) Multi-level magma plumbing at Agung and Batur volcanoes increases risk of hazardous eruptions. *Sci Rep* 8:10547
- Gonnermann HM, Manga M (2013) Dynamics of magma ascent in the volcanic conduit. In: Fagents SA, Gregg TKP, Lopes RMC (eds) *Modeling Volcanic Processes: The Physics and Mathematics of Volcanism*. Cambridge University Press, pp 55–84
- Halldórsson SA, Marshall EW, Caracciolo A, Matthews S, Bali E, Rasmussen MB, Ranta E, Gunnarsson Robin J, Guðfinnsson GH, Sigmarsson O, MacLennan J, Jackson MG, Whitehouse MJ, Jeon H, van der Meer QHA, Mibei GK, Kalliokoski MH, Repczynska MM, Hlín Rúnarsdóttir R et al (2022) Rapid shifting of a deep magmatic source at Fagradalsfjall volcano, Iceland. *Nature* 609:529–534
- Hamada M, Kawamoto T, Takahashi E, Fujii T (2011) Polybaric degassing of island arc low-K tholeiitic basalt magma recorded by OH concentrations in Ca-rich plagioclase. *Earth Planet Sci Lett* 308(1–2):259–266
- Hartley ME, Thordarson T (2013) The 1874–1876 volcano-tectonic episode at Askja, North Iceland: lateral flow revisited. *Geochem Geophys Geosyst* 14(7):2286–2309
- Hauri EH, Gaetani GA, Green TH (2006) Partitioning of water during melting of the Earth's upper mantle at H₂O-undersaturated conditions. *Earth Planet Sci Lett* 248(3–4):715–734
- Hercule S, Ingrin J (1999) Hydrogen in diopside: diffusion, kinetics of extraction-incorporation, and solubility. *Am Mineral* 84:1577–1587
- Holloway JR, Blank JG (1994) Application of experimental results to C-O-H species in natural melts. *Rev Mineral Geochem* 30:187–230
- Ingrin J, Blanchard M (2006) Diffusion of hydrogen in minerals. *Rev Mineral Geochem* 62:291–320
- Ingrin J, Skogby H (2000) Hydrogen in nominally anhydrous upper-mantle minerals: concentration levels and implications. *Eur J Mineral* 12(3):543–570
- Johnson ER, Wallace P, Cashman KV, Granados HD (2010) Degassing of volatiles (H₂O, CO₂, S, Cl) during ascent, crystallization, and eruption at mafic monogenetic volcanoes in central Mexico. *J Volcanol Geotherm Res* 197(1–4):225–238
- La Spina G, Arzilli F, Burton MR, Polacci M, CA B (2022) Role of volatiles in highly explosive basaltic eruptions. *Communications Earth & Environment* 3(156)
- Lange RA, Frey HM, Hector J (2009) A thermodynamic model for the plagioclase-liquid hygrometer/thermometer. *Am Mineral* 94(4):494–506
- Libowitzky E, Rossman GR (1997) An IR absorption calibration for water in minerals. *Am Mineral* 82(11–12):111–1115
- Lloyd AS, Ferriss E, Ruprecht P, Hauri EH, Jicha BR, Plank T (2016) An assessment of clinopyroxene as a recorder of magmatic water and magma ascent rate. *J Petrol* 57(10):1865–1886
- Lucic G, Berg A-S, Stix J (2016) Water-rich and volatile-undersaturated magmas at Hekla volcano, Iceland. *Geochem Geophys Geosyst* 17(8):3111–3130
- Malfait WJ, Seifert R, Petitgirard S, Mezouar M, Sanchez-Valle C (2014) The density of andesitic melts and the compressibility of dissolved water in silicate melts at crustal and upper mantle conditions. *Earth Planet Sci Lett* 393:31–38
- Marti J, Folch A (2005) Anticipating volcanic eruptions. In: Marti J, Ernst GGJ (eds) *Volcanoes and the environment*. Cambridge University Press, pp 99–120
- Métrich N, Berry AJ, O'Neill HSC, Susini J (2009) The oxidation state of sulfur in synthetic and natural glasses determined by X-ray absorption spectroscopy. *Geochim Cosmochim Acta* 73:2382–2399
- Métrich N, Wallace P (2008) Volatile abundances in basaltic magmas and their degassing paths tracked by melt inclusions. *Rev Mineral Geochem* 69(1):363–402
- Michael PJ, Schilling J-G (1989) Chlorine in mid-ocean ridge magmas: evidence for assimilation of seawater-influenced components. *Geochim Cosmochim Acta* 53:3131–3143
- Mollo S, Putirka KD, Misti V, Soligo M, Scarlato P (2013) A new test for equilibrium based on clinopyroxene–melt pairs: clues on the solidification temperatures of Etnean alkaline melts at post-eruptive conditions. *Chem Geol* 352:92–100
- Moore G, Vennemann T, Carmichael ISE (1998) An empirical model for the solubility of H₂O in magmas to 3 kilobars. *Am Mineral* 83:36–42
- Morimoto N (1988) Nomenclature of pyroxenes mineralogy and petrology 39:55–76
- Moussallam Y, Oppenheimer C, Scaillet B, Gaillard F, Kyle P, Peters N, Hartley ME, Berlo K, Donovan A (2014) Tracking the changing oxidation state of Erebus magmas, from mantle to surface,

- driven by magma ascent and degassing. *Earth Planet Sci Lett* 393:200–209
- Nazzareni S, Rossi S, Petrelli M, Caricchi L (2020) Architecture of the magmatic system in the main Ethiopian rift. In: Vetere F (ed) *Dynamic Magma Evolution*. American Geophysical Union
- Neave DA, Putirka KD (2017) A new clinopyroxene-liquid barometer, and implications for magma storage pressures under Icelandic rift zones. *Am Mineral* 102:777–794
- Nichols ARL, Carroll MR, Höskuldsson A (2002) Is the Iceland hot spot also wet? Evidence from the water contents of undegassed submarine and subglacial pillow basalts. *Earth Planet Sci Lett* 202:77–87
- Nikkola P, Bali E, Kahl M, Van der Meer QHA, Rämö OT, Guðfinnsson GH, Thordarson T (2019) Mid-crustal storage and crystallization of Eyjafjallajökull ankaramites, South Iceland. *Jökull* 69:77–96
- O’Leary JA, Gaetani GA, Hauri EH (2010) The effects of tetrahedral Al³⁺ on the partitioning of water between clinopyroxene and silicate melt. *Earth Planet Sci Lett* 297:111–120
- Passmore E (2009) Feeding large eruptions: crystallisation, mixing and degassing in Icelandic magma chambers. University of Edinburgh
- Pedersen GBM, Belart JMC, Óskarsson BV, Guðmundsson MT, Gies N, Högnadóttir T, Pinel V, Berthier E, Dürig T, Reynolds HI, Hamilton CW, Valsson G, Einarsson P, Ben-Yehosua D, Gunnarsson A, Oddsson B (2021) Volume, effusion rate, and lava transport during the 2021 Fagradalsfjall eruption: results from near real-time photogrammetric monitoring. *Earth and Space Science Open Archive* 20
- Petrelli M, El Omari K, Spina L, Le Guer Y, La Spina G, Perugini D (2018) Timescales of water accumulation in magmas and implications for short warning times of explosive eruptions. *Nat Commun* 9(770)
- Polacci M, Corsaro RA, Andronico D (2015) Coupled textural and compositional characterization of basaltic scoria: insights into the transition from Strombolian to fire fountain activity at Mount Etna. *Italy Geol* 34(3):201–204
- Poreda R, Schilling J-G, Craig H (1986) Helium and hydrogen isotopes in ocean-ridge basalts north and south of Iceland. *Earth Planetary Sci Lett* 78:1–17
- Preece K, Gertisser R, Barclay J, Charbonnier SJ, Komorowski J-C, Herd RA (2016) Transitions between explosive and effusive phases during the cataclysmic 2010 eruption of Merapi volcano, Java. *Indonesia Bull Volcanol* 78(54)
- Putirka KD (2008) Thermometers and barometers for volcanic systems. *Rev Mineral Geochem* 69:61–120
- Putirka KD, Johnson M, Kinzler R, Longhi J, Walker D (1996) Thermobarometry of mafic igneous rocks based on clinopyroxene-liquid equilibria, 0–30 kbar. *Contrib Mineral Petrol* 123:92–108
- Roggensack K, Hervig RL, McKnight SB, Williams SN (1997) Explosive basaltic volcanism from Cerro Negro Volcano: influence of volatiles on eruptive style. *Science* 277(5332):1639–1642
- Sæmundsson K (2016) Geological map of Southwest Iceland, 1:100000. Iceland GeoSurvey
- Sides IR, Edmonds M, MacIennan J, Swanson DA, Houghton BF (2014) Eruption style at Kīlauea Volcano in Hawai‘i linked to primary melt composition. *Nat Geosci* 7:464–469
- Sigmundsson F, Pinel V, Grapenthin R, Hooper A, Halldórsson SA, Einarsson P, Ófeigsson BG, Heimisson ER, Jónsdóttir K, Guðmundsson MT, Vogfjörð K, Parks M, Li S, Drouin V, Geirsson H, Dumont S, Fridriksdóttir HM, Guðmundsson GB, Wright TJ, Yamasaki T (2020) Unexpected large eruptions from buoyant magma bodies within viscoelastic crust. *Nat Commun* 11
- Skogby H (2006) Water in natural mantle minerals I: pyroxenes. *Rev Mineral Geochem* 62:155–167
- Skogby H, Bell DR, Rossman GR (1990) Hydroxide in pyroxene: variations in the natural environment. *Am Mineral* 75(7–8):764–774
- Skogby H, Rossman GR (1989) OH⁻ in pyroxene: an experimental study of incorporation mechanisms and stability. *Am Mineral* 74:1059–1069
- Stalder R, Ludwig T (2007) OH incorporation in synthetic diopside. *Eur J Mineral* 19:373–380
- Sundvall R, Skogby H, Stalder R (2008) Dehydration-hydration mechanisms in synthetic Fe-poor diopside. *Eur J Mineral* 21(1):17–26
- Tenzer R (2013) Global model of the upper mantle lateral density structure based on combining seismic and isostatic models. *Geosciences Journal* 17(1):65–73
- Wade JA, Plank T, Hauri EH, Kelley KA, Roggensack K, Zimmer M (2008) Prediction of magmatic water contents via measurement of H₂O in clinopyroxene crystals. *Geology* 36(10):799–802
- Wallace P, Plank T, Edmonds M, Hauri EH (2015) Volatiles in magmas. In: Sigurdsson H (ed) *The Encyclopedia of volcanoes*. Academic Press, pp 163–183
- Weis FA, Skogby H, Troll VR, Deegan FM, Dahren B (2015) Magmatic water contents determined through clinopyroxene: examples from the Western Canary Islands, Spain. *Geochem Geophys Geosyst* 16(7):2127–2146
- Woods AW, Koyaguchi T (1994) Transitions between explosive and effusive eruptions of silicic magmas. *Nature* 370:641–644
- Woods SC, Mackwell S, Dyar D (2000) Hydrogen in diopside: diffusion profiles. *Am Mineral* 85(3):480–487